DRAFT VERSION DECEMBER 10, 2020
Typeset using LaTeX **twocolumn** style in AASTeX61

MAPPING GALACTIC DISK OSCILLATIONS IN M GIANTS WITH GAIA DR2

ANASTASIOS TZANIDAKIS[1]

[1]*Department of Astronomy, Columbia University, 116th St and Broadway, New York, NY 10027, USA*

ABSTRACT

Recent astrometric surveys have traced halo overdensities that resemble arc-like features around the outer disk of the Milky Way. Such features appear in stellar count maps as concentric arcs toward the Galactic Anticenter and are found above and below the midplane. Yet, due to their large heliocentric distances, these crucial parts of the Milky Way have not been fully mapped in phase-space. Previous studies have shown many of these features have stellar populations consistent with those of the Galactic disk. Likewise, N-body simulations of a Milky Way-like disk interacting with a Sagittarius-like dwarf-spheroidal (dSpH) galaxy have shown the dSph's ability to dynamically perturb the disk, causing density fluctuations at large and small scales. We trace these features with a photometric selection of M giant stars observed with *Gaia* DR2, deriving their distance via a color-metallicity relation. Preliminary results find that in Galactic coordinates $100<\ell$ [*deg*]<160 and $70<b$ [*deg*]<-70 substructure emerges in number of star count in bins of distance modulus. Our data suggest that there exists overall a greater number of M Giants above the Galactic plane. Recent discussion about the impact of massive dwarf spheroidal galaxies have on Galactic disk suggest the presence of global oscillations about the midplane. We confirm that these substructures are found at distances beyond $d_{helio}>14 \pm 5$ kpc within the *Gaia* DR2 catalog. While spatially we have confirmed the existence of overdense regions, to draw stronger conclusions, future work should attempt to map the proper motions of such regions to determine the overall the full phsase-space. With *Gaia* DR3 and LSST in the near future, the the detailed mapping of these features will reveal the evolution and global morphology of the Milky Way.

Keywords: Milky Way Disk, Galactic Oscillations, Galaxies, Stellar Populations

1. BACKGROUND

With the advent of all-sky surveys, the outskirt of the Galactic disk has revealed a variety of complex substructure (Slater et al. 2014). For almost two decades, there has been a long-lasting debate about the morphology of the Galactic disk and the dynamic consequences of merging dwarf satellite galaxies onto the disk (Weinberg 1995; Ibata 1998). The idea of disk oscillations, became most prominent around 2012 when a group of researchers found that stars in the solar neighborhood exhibited oscillatory-like features by looking at bulk-motions and density profiles of stars around the sun (Widrow et al. 2012). The consequences of such finding, re-kindled a debate about the true morphology of the disk, with studies suggesting that perhaps the most massive dwarf satellite galaxy currently undergoing tidal disruption, Sagittarius (Ibata et al. 1994), could be the leading cause of such asymmetries in the Galactic disk (Ibata; Razoumov 1998; Dehnen 1998; Laporte et al. 2017). However, at the time it was unknown to what extent did these oscillations carry out, as the connections remained unclear. Things for the Galactic Archaeology community began to gain more momentum, with the discussion and the increased discovery of diffuse stellar substructures (Majewski al. 2004; Rocha-Pinto et al. 2004; Martin et al. 2007; Sheffield et al. 2014; Li et al. 2017). The puzzle came together with mounting evidence from observations that demonstrated that most of these substructures contained stars that were originally formed in the disk of the Milky Way that have been "kicked-out" due to dynamical perturbations (Price-Whelan et al. 2015; Sheffield et al. 2018; Laporte et al. 2018; Bergemann et al. 2018) most likely by Sagittarius dwarf spheroidal galaxy.

Inspired by the recent work to trace substructure in the outer disk with M Giants (Sharma et al. 2010; Sheffield et al. 2014; Li et al. 2017), this work attempts to recreate such results using the *Gaia* DR2 catalog. By identifying substructure with the *Gaia* DR2 catalog, it is possible that the use of proper motion can better help constrain the bulk-motion and distribution of such overdensities. For example, a fully mapped phase-space view of substructures can refine our theoretical understanding of dynamical models of the Galactic disk (Johnston et al. 2017). In this analysis, we report the number of M Giant stars in bins of distance modulus (μ) and metallicity coverage [Fe/H] of M Giant stars in the regions span by $100<\ell$ $[deg]<160$ and $70<b$ $[deg]<-70$. In Section 2, we discuss the methods of querying the *Gaia* DR2 catalog, selecting a pure sample of M Giants, estimating contamination rates of M Dwarfs, and determining the absolute magnitudes of M Giants. In Section 3, we elaborate on the number of stars as a function of distance modulus, estimate the ratios of M Giants identified between $-35<b$ $[deg]<-15$ and $15<b$ $[deg]<35$ and subtract the number of M Giants identified at $|b|>10$. Finally, our conclusions and implications of our analysis are presented in Section 4.

2. METHODS

2.1. *Gaia DR2 and Two-Micron-All-Sky-Survey Catalogs*

Our motivation to use *Gaia* DR2 is to determine whether it is possible to trace large-scale oscillations in the Galactic disk beyond the solar neighborhood and draw any conclusions upon its morphology. With the advent of *Gaia* DR2, we now have the position, parallax (ω), and proper motions of over 1.3 billion stars (*Gaia* Collaboration 2018). *Gaia* DR2 has already has begun to change our understanding of the Galactic disk by revealing rich substructure (Antoja et al. 2018). Recent work using *Gaia* DR2 conducted by Bennett and Jovy (2018) confirmed that the local solar neighborhood exhibits density and velocity fluctuations consistent with an oscillating disk. Such results may signal oscillations carried out beyond the solar neighborhood.

In this study, we query the *Gaia* DR2 catalog spanned by Galactic coordinates $160^o<\ell$ $[deg]<100^o$ and $-70^o<b$ $[deg]<70^o$ where the majority of substructures found at high Galactic latitudes have been identified as members of the Galactic disk (see Price-Whelan et al. 2015, Sheffield et al. 2018, Bergemann et al. 2018). Since the majority of the M Giants will be selected based on their associated 2MASS magnitudes (see Section 2.2) we place no limit on parallax, proper motion, and magnitude in our *Gaia* DR2 query. Instead, we follow the data filtering procedure highlighted in the *Gaia* Collaboration 2018 that removes sources with poor astrometric estimates. Since M Giant stars are cool and luminous sources, we specifically need colors such as $(J-H)$ and $(J-K_s)$ that are most sensitive to the near infra-red that are optimal for selecting (Li et al. 2016). Thus by first querying and filtering the *Gaia* DR2 data, we then crossmatch the sources via their associated 2MASS ID, with a final sample size of $N = 343,146$ M giants.

2.2. *M Giant Selection with 2-Micron-All-Sky-Survey*

One of the many advantages of using M Giant stars is that they can be traced at distances up to 100 kpc (Majewski et al. 2003) and overall trace inherently metal-rich regions in the Galaxy (Sharma et al. 2010) thus making them good candidates associated with the Galactic disk. Prior to selecting M Giants in our *Gaia*/2MASS (G2M) sample, we need to account for dust rendering of our sources in the 2MASS color system, K_s, J and H magnitudes. We dereddened our sample using the 3D Batestar17 dust maps highlighted in Green et al. 2015, and extinction coefficients, R_{Ks}, R_J, R_H outlined by Yuan et al. 2013 Table 2. The intrinsic and dereddened magnitudes will be denoted as Ks_0, J_0 and H_0.

To select a pure sample of M Giant stars, we choose to follow the methods highlighted in Sharma et al. 2010 using 2MASS photometric color-magnitude cuts given by the following relationships:

$$4 < K_{s0} < 12 \tag{1}$$

$$(J-K_s)_0 > 0.85 \tag{2}$$

$$(J-H)_0 < 0.56(J-K_s)_0 + 0.36 \tag{3}$$

$$(J-H)_0 > 0.56(J-K_s)_0 + 0.19 \tag{4}$$

While the used photometric selection functions will successfully identify most M giant stars, a small fraction of those will be M dwarfs, since M Dwarfs and M Giants begin to separate at $(J-K_s)_0$>0.95 (Sharma et al. 2010).

Alternative methods to set apart M Dwarfs from M Giants could be found based on their relative absorption line strength of the Na I doublet (Schiavon et al. 1997). Since our original G2M sample does not contain high-resolution spectra, we probe the number of contaminants using a synthetic stellar population generator, the GALAXIA model (see Sharma et al. 2011). Using the same photometric and Galactic coordinate projection cuts for our G2M sample, we apply those same parameters to GALAXIA to generate the distribution of M Giant stars in the stellar disk.

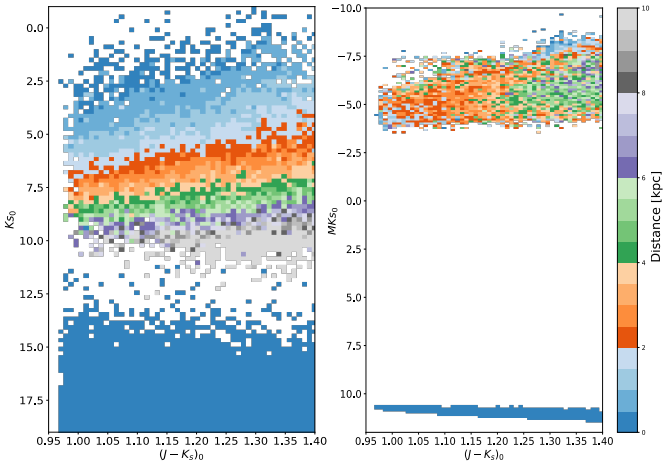

Figure 1. The left panel represents the color-magnitude relation between the generated M Giant Stars from GALAXIA colorcoded by heliocentric distance. On the right, we plot the absolute magnitude-color relation of GALAXIA stars colorcoded by the heliocentric distance.

Figure 1 represents the synthetic stellar population given by GALAXIA in M Dwarfs and M Giants using the suggested photometric cuts by Sharma et al. 2010. Seen immediately in the right panel of Figure 1 is the emergence of two separate stellar sequences. The one sequence of M Dwarfs (for values MKs_0>10) for which the majority lies within d_{helio}<2 kpc, and M Giants (for values MKs_0<-2.5) for d_{helio}>2 kpc. Similarly, on the right panel of Figure 1 we can also see that there exists a separation between the two sequences, but much closer in magnitude. We note that almost all M Dwarfs are less than 1 kpc from the Sun, thus this demonstrates with a simple parallax cut of approximately <2 kpc at most, if not all M Dwarf contaminants should not be part of our G2M sample. Our synthetic population of M Giants demonstrates that for a stellar disk spanned by $R \approx 10$ kpc, most M Dwarfs separated in both absolute and apparent magnitude $Ks0$ and MKs_0. To further ensure that the number of contaminants is at a minimum, we also place a cut-off magnitude limit to our sample of Ks_0<12, which should also remove any residual M Dwarfs that may be found very close to the Sun. Ultimately, such an approach suggests a quick and reliable method of collecting a pure sample of M Giants with a very small contamination number of M dwarfs.

2.3. *Calculating Absolute Magnitudes of M Giants*

Another useful relationship of M Giants that allows estimates on distances is due to their linear relation between Ks_0, $(J-K_s)_0$ and $[Fe/H]$ (see Equation 2, Sheffield et al. 2014). More generally, such relation could be broadly written in terms of its coefficients (C_0, C_1, C_2):

$$M_{K_s} = C_0 + C_1[Fe/H] + C_2(J-K_s) \tag{5}$$

It is often that astrometric catalogs (i.e *Gaia* DR2) contain very little information on the spectroscopic information of sources. Further, one of the disadvantages of exploring the Galactic Anticenter is the lack of incompleteness of [Fe/H] measurements for the Galactic coordinates where disk substructures are found (Majewski et al. 2015). Instead, one way to work around our estimates of the metallicity of M Giants, we turn to current catalogs that contain large volumes of spectroscopic information analogous to our G2M sample.

As a separate analysis, we utilize spectroscopic data from the Sanders and Das 2018 (see Sanders & Das 2018) catalog (hereafter SD), which contains spectroscopic information of nearly 3 million stars from *Gaia* DR2 crossmatched with large spectroscopic surveys (e.g. APOGEE, RAVE). Using the same method described in Section 2.2, we can re-apply the M Giant selection functions and extinction corrections to select only M giant stars from the SD catalog for the entire Anticenter. As seen in Figure 2, it is evident that there exists a metallicity dichotomy between metal-rich M Giants close to the Galactic midplane versus those metal-poor at higher Galactic latitudes. It is important to note that since M Giants are rare (Sharma et al. 2010), the sample size of the SD catalog has decreased to only a few thousand stars in the regions

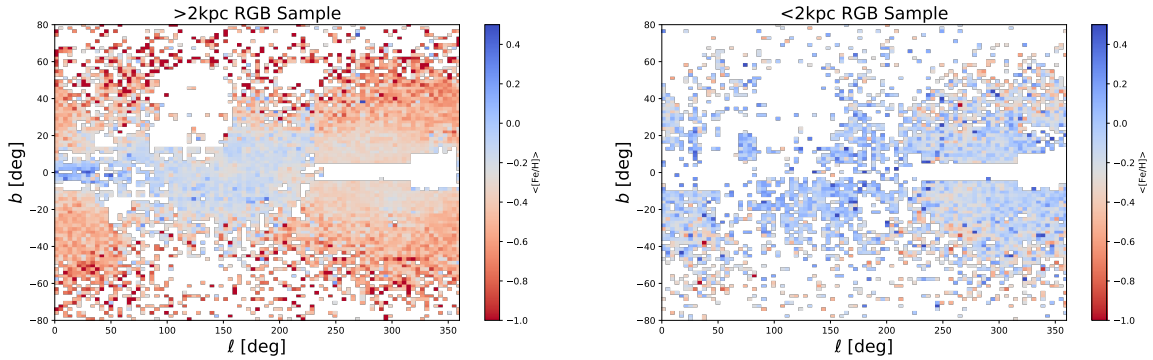

Figure 2. Galactic coordinate projections (ℓ, b) colorcoded by median metallicity per 10 deg^2 bins (<[Fe/H]>) from SD M Giant catalog. The left figure shows the sky distribution of M Giants at d_{helio}<2kpc using ω>0.5mas. Similarly, the right panel shows the M Giant sky distribution at d_{helio}>2kpc with 0 mas <ω <0.5 mas.

of this study. Furthermore, we can see that the coverage of spectroscopic information is not uniform, especially for the sample that is located beyond the 2 kpc distance range.

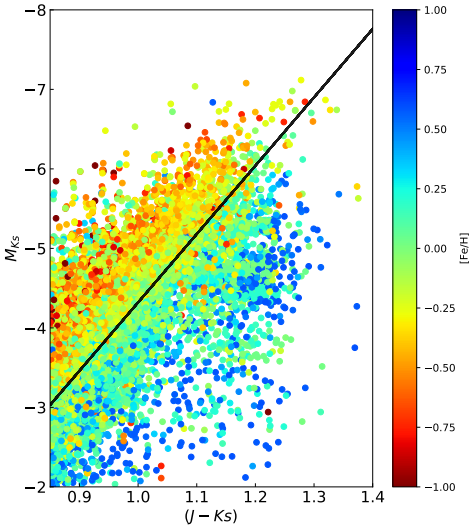

Figure 3. Absolute magnitude as a function of 2MASS color $(J-K_s)_0$ colorcoded by [Fe/H] from SD catalog (see Section 2.2) for local solar neighbourhood of M Giants. The black solid line represents the best fit linear model (see Equation 5).

To account for the lack of spectroscopic data, we use the more complete sample that is less than d_{helio}<2 kpc, which contains roughly a Gaussian distribution of metallicity with $\mu_{[Fe/H]} \approx -0.6$. To apply Equation 5 to our original G2M sample, we first need to estimate the coefficients (C_0, C_1, C_2) the linear relationship and compare them to those found by Sheffield et al. 2014. Since the SD sample contains enough spectroscopic information, we perform a Least-Squares fit (seen in Figure 3) to the color-magnitude diagram using Equation 5. Due to the large scatter in M_{Ks} and potential outliers, we performed a 2-σ clip prior to our fit. Our results for C_0, C_1 and C_2 are nearly similar to those reported in Sheffield et al. 2014, however with a slight offset in the C_0 term which is caused most likely due to our parallax filter (ω>0.5 mas). Since the SD sample considers only within M Giants within the solar neighborhood, we expect that at larger distances the scatter will increase and thus the value C_0. In conclusion, our values have agreed with the reported constants, and for our color-magnitude-metallicity relation, we adopt the coefficient constants to those reported by Sheffield et al. 2014.

Last, since our G2M catalog will not contain any prior spectroscopic information we choose to investigate if there exist any obvious gradients in metallicity as a function of our given variables, such as Ks_0. As expected, Figure 3 demonstrated that there is indeed an empirical relation (Equation 5) between the metallicity, absolute magnitude, and color. However, we found that this gradient is smeared when we plot the metallicity as a function of apparent magnitude. To ensure that there was no associated metallicity-apparent magnitude relation, we binned the metallicity and apparent magnitude, applied a running median, and found that the slope was nearly zero and our line was held at a constant value of [Fe/H]=-0.27±0.35. Using all the information acquired from the SD catalog, we substitute all constant values as:

$$M_{Ks_0} = 3.81 + 1.32(-0.27 \pm 0.35) - 8.4(J-K_s)_0 \qquad (6)$$

Due to the high dispersion in our [Fe/H] substitute, Equation 5 will have an estimated uncertainty of 35% for distances up to $d_{helio} \approx 35$ kpc. Before applying our newly refined model (Equation 6), we clip $(J-K_s)_0$<1.4 to avoid any extreme values that our model may estimate.

3. DISCUSSION

3.1. *Distance Modulus Star Count Maps*

To explore substructure in the Galactic disk we estimate the distance modulus $\mu = Ks_0$-M_{Ks_0} of each star by adopting Equation 6 (see Section 2.3) to the G2M data. The specific

sky projection that our G2M data spans can be assumed to be full of substructure (Sheffield et al. 2014, Xu et al. 2015). Figure 4 exhibits the number of M Giants binned in distance modulus with the associated standard error and uncertainty from Equation 6. We can see that immediately it reveals just a little beyond $\mu \approx 14.7$, equivalent to about 10-13 kpc from the Sun, a flattening in numbers of stars suggesting an overdense region at a Galactic latitude 15< b [deg]<35. The highlighted green region shades the approximate rough distance that the Monoceros substructure has been previously identified by Newberg et al. 2002.

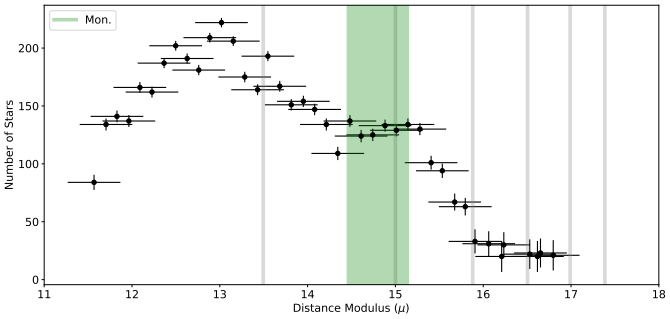

Figure 4. Number of stars as a function of distance modulus for 35>b [deg]>15. Each solid grey line represents the distance modulus converted to a heliocentric distance in increments of 5kpc. The shaded green region highlights the identified Monoceros substructure.

On the other hand, Figure 5 represents the number of M Giant stars as a function of distance modulus below the Galactic midplane at Galactic latitude -35<b[deg]<-15. Among the selected fields, this region of the Galaxy exhibits a richness in the substructure. The first feature emerges in Figure 5 at $\mu \approx 13.5$ with a small flattening in the number of stars. The highlighted regions in Figure 5 (yellow and red) are the regions where previous literature has reported substructure: TriAnd-1 and TriAnd-2 (Sheffield et al. 2014). It is interesting to note that for TriAnd-1 and TriAnd-2, each structure is spanned only by a distance modulus of $\delta\mu \approx 0.5$ which is approximately 4 kpc. Given our relative high uncertainty, if indeed the distance is so small this could perhaps indicate that TriAnd-1 and TriAnd-2 are part of the same substructure and suggest that it extends much further than previously thought. Alternatively, considering that there are roughly 2 bins with 30 M Giants per bin, it is likely that this is a signature of a third substructure. Nonetheless, it is evident that prior to the TriAnd substructures the number of stars profile drops in number faster in contrast to the M Giants above the midplane of the Galaxy.

Figure 6 attempts to quantitatively answer such asymmetry between the upper and lower projection of the midplane, called here the North-South asymmetry. In the top panel of Figure 6, each distance modulus begins with an expected in-

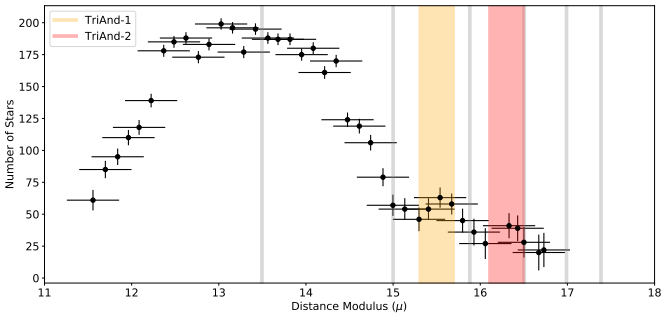

Figure 5. Number of stars as a function of distance modulus for -35<b[deg]<-15. Each solid grey line represents the distance modulus converted to a heliocentric distance in increments of 5kpc. The shaded red and orange regions highlight the identified TriAnd-1 and TriAnd-2 substructures.

crease number of stars for small distance modulus μ with roughly the same number-count. Interestingly, at $\mu \approx 14$ the red data points seem to succeed the count while there is a subtle small dip for the black points, then we have the next overdense region (Monoceros) $\mu \approx 15$ which the reversed pattern of underdense-overdense. The lower panel reveals the percent change from the North-South asymmetry. The spike at $\mu \approx 15$ suggests that the upper midplane has twice more M giants than those of the lower midplane and for the earlier $\mu \approx 14$ the south is only a few number stars more than the upper half. Curiously, such a pattern resembles fluctuations in density similar to those of a kind of wave-like oscillation (Li et al. 2017).

3.2. *Comparison with N-Body Simulations*

One method of interpreting such fluctuations in number-count, we can compare our results in an isolated environment such as that of N-body simulations. We use a high-resolution N-body simulation Milky Way-like Galaxy interacting with a Sagittarius-like (Sgr) dwarf spheroidal galaxy (dSph) with initial mass $10^{11} M_{\odot}$ (see Laporte et al. 2017). During its interaction with the disk, Sgr makes 5 pericentric passages through the disk, ejecting particles at extreme Galactic latitude such as those found in this study. Furthermore, in Laporte et al. 2018 it was demonstrated that the disk interacting with Sgr dSph is capable of producing substructures similar to those observed in the PanSTARSS maps by Slater et al. 2014 (Laporte et al. 2018 and Sheffield et al. 2018).

To simulate the distance modulus for each snapshot in the N-body simulation, we assume that each distance is known and that the Ks_0 magnitude is approximately distributed as $\mathcal{N}(\mu_{Ks_0,\sigma_{Ks_0}})$ with $\mu_{Ks_0,\sigma_{Ks_0}}$ values derived from our G2M sample. We can further assume that distance modulus uncertainty will be similar to that of the data. As demonstrated

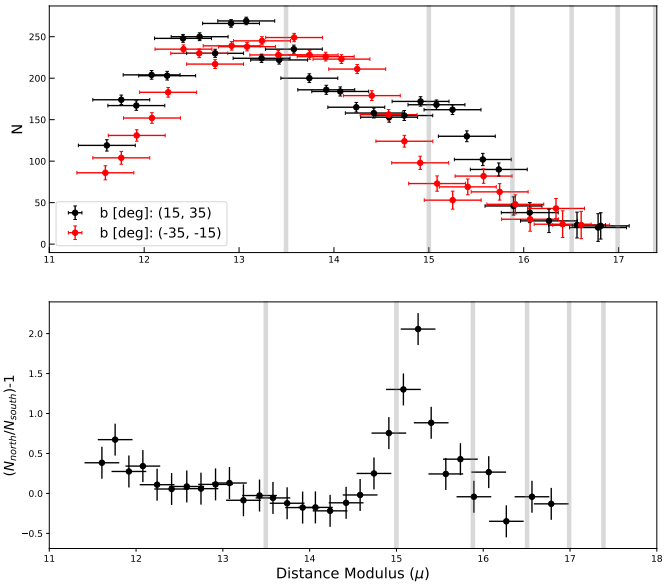

Figure 6. Top panel shows the number of stars a function of distance modulus for North (b [deg]>0) and South (b [deg]<0) projections of M Giants stars with the G2M sample. Lower panel shows the ratio or percent change between the two projections for each distance modulus bin.

in Figure 7, we can see the case of $\tau \approx 1 Gyr$ where Sgr has not yet impacted the disk, generally, the simulated distance modulus of the particles will be distributed as a Gaussian. In contrast, $\tau \approx 5.56 Gyr$ after Sgr has made several pericentric passages, we can see such large-scale amplitudes in number-count at distances of approximately 25-30 kpc from the sun. It is worthy that the amplitudes in overdensity we see in the N-body simulations should not match exactly to that seen in the data. Instead, we choose to make such a comparison to demonstrate that if such a physical process took place, the overall shape and distribution of distance modulus of stars would take on abrupt peaks and drops in star-count.

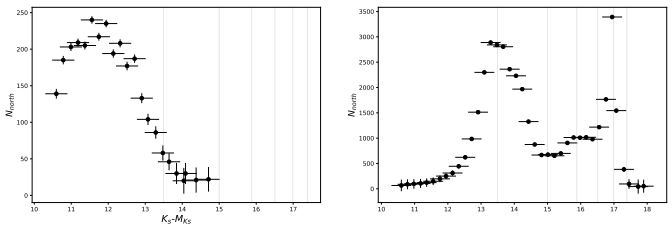

Figure 7. Left panel represents number of stars as a function of distance modulus for an N-body simulation (Laporte et al. 2018) at $\tau \approx 1 Gyr$. Analogously, the right figure shows the same same N-body simulation at $\tau \approx 5.56 Gyr$.

Another promising consistency with our data is that in comparison to the work reported by Xu et al. 2015, where such asymmetries in star-count as a function of distance was presented in Main-Sequence in similar regions conducted in this analysis. Perhaps one future question to be asked is if there is a discrepancy between the asymmetry of Main-Sequence to M Giants and if it could signify the period of such oscillations.

3.3. *Bulk Distribution of M Giants Above the Galactic Midplane?*

Since our analysis sets no prior on distance, the expected error in distance derived from our work would limit our interpretation beyond d_{helio}>15 kpc. In the original analysis of the SD catalog, Sanders and Das et al. 2018 derive distances by the deployment of a Bayesian framework (see Sanders and Das et al. 2018) with uncertainties to Giants of about 20%. In Figure 8, we plot the 3D physical coordinates (X,Y) of stars between: 90<ℓ [deg]<180 and $|b[deg]|$>10. Color-coded we have plotted the difference in $Z_{b>10}$ - $Z_{b<-10}$, to display any differences in number-count above and below the midplane. Indecently the distance where we identify the Monoceros substructure, we convert their approximate distances in physical coordinates and overlay it on Figure 8 (seen in black scatter). As shown in Figure 4, the signature of the Monoceros substructure overall dominates the substructures below b [deg]<0.

The difference between the number of M Giants found on the upper-half and lower-half of the disk indicates that overall, between 90<ℓ [deg]<180 M Giants are predominantly found above the midplane with a flaring like morphology (see Feast et al. 2014) at $R \approx 12 kpc$. In a study conducted by Laporte et al. 2017, they showed an N-body simulation of a Milky Way-like galaxy interacting with a Sagittarius-like dwarf spheroidal galaxy including the Large Magellanic Cloud, can similarly produce an oscillating disk. Moreover, they also find a similar quality of gradual flare at radii of R = 15 kpc and R = 20 kpc (Laporte et al. 2017) This statement, however, is taken with caution, since our bin completeness beyond 10 kpc is relatively low and thus not capable of making any definite conclusion.

4. CONCLUSIONS

The results presented in this analysis suggest a preliminary view of an oscillating Galactic disk beyond d_{helio}>10 kpc. We have confirmed using photometric selections of M Giant stars with 2MASS that stars above and below the midplane of the galaxy exhibit an asymmetry in number, with the most prominent signal at a distance modulus $\mu \approx 15$. We also find that the Galactic projection 100<ℓ [deg]<160 and -35<b [deg]<-15 emerge three substructures, of decreasing amplitude as a function of distance modulus. Using the distances reported by Sanders and Das et al. 2018 we find that for a span of $\delta\ell$ = 90 deg (90<ℓ [deg]<180 and $|b|$>10 deg) M Giant stars identified in the SD catalog exhibit an overall flare-like feature above the Galactic midplane consistent

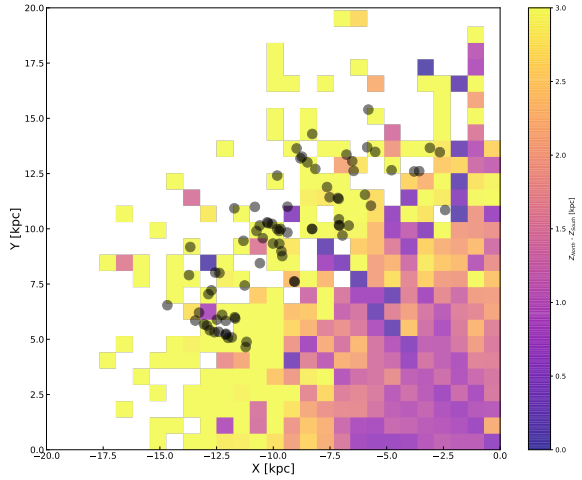

Figure 8. SD sample of M Giant stars in physical coordinates (X,Y) in bins of 0.7 kpc^2 and colorcoded by the difference in $Z_{b>10}$ - $Z_{b<-10}$ in units of kpc. Black scatter highlight the physical position and distance span of the Monoceros substructure. The Sun is located at X=Y=0 [kpc] with a radius of 8.2 kpc and height above the plane at 15 parsecs (Bland-Hawthorn and Gerhard 2016)

with the position of the Monoceros substructure. This analysis also confirmed that such stars exist within the *Gaia* DR2 catalog.

In future work, we aim to explore the proper motions of such distance modulus bins to examine the presence or absence of vertical velocity asymmetries. With the aid of proper motion, our understanding of disk oscillations and flares will expand and place better constraints on theoretical models of the Galactic disk (Johnston et al. 2017). Another interesting question to examine is to compare the amplitudes of the North-South asymmetry for various stellar populations. If such a method were to succeed, speculatively the age of oscillations can be linked to the pericentric passage of Sgr. Ultimately, together with an understanding of the spatial distribution and velocities, we ask if such oscillations are present, and how do they propagate as a function of Galactic radius.

5. ACKNOWLEDGEMENTS

I thank my research mentors Kathryn Johnston, Allyson Sheffield, Chervin Laporte, and Adrian Price-Whelan for their unconditional commitment to guide and mentor me through the fascinating field of Galactic Archaeology and advise with the project. I also would like to thank Marcel Agüeros for his constructive feedback and support in making this project possible. This research was conducted under a two-semester term, Independent Research Class UN3998 advised by Marcel Agüeros at Columbia University, New York. This work has made use of data from the European Space Agency (ESA) mission *Gaia*, and data products from the Two Micron All Sky Survey. This research was partially supported by the NSF grant AST - 1614743. Dedicated to Lily.

REFERENCES

Antoja T., Helmi A., Romero-Gòmez M., Katz D., et al., 2018, Nature, 561, 360
Bergemann, M., Sesar, B., Cohen, J. G., et al. 2018, Nature, in press
Bland-Hawthorn J., Gerhard O., 2016, ARAA, 54, 529 Nature, in press
Dehnen W., 1998, AJ, 115, 2384
Feast M. W., Menzies J. W., Matsunaga N., Whitelock P. A.,2014, Nature, 509, 342
Green, G. M., Schlafly, E. F., Finkbeiner, D. P., et al. 2015, ApJ, 810, 25
Gaia Collaboration, Babusiaux, C., van Leeuwen, F., et al. 2018a, AA, 616, A10
Ibata R. A., Gilmore G., Irwin M. J., 1994, Nature, 370, 194
Ibata R. A., Razoumov A. O., 1998, AAP, 336, 130
Johnston, K. V., Price-Whelan, A. M., Bergemann, M., et al. 2017, Galaxies, 2, 410
Katz D., Antoja T., Romero-Gòmez M., Drimmel R. et al. 2018, Gaia
Laporte C.F.P, Johnston K.V, Gòmez A.F et al. 2018, MNRAS, 481
Li T. S., Sheffield A. A., Johnston K. V., et al. 2017, ApJ, 844, 74
Li, J., Smith, C. M., Zhong, J., et al. 2016, ApJ, 59, 149
Majewski, S. R., Skrutskie, M. F., Weinberg, M. D., Ostheimer, J. C. 2003, ApJ, 599, 1082
Majewski, S. R., Schiavon,R. P., Frinchaboy, P. M., et al., 2015, ApJ, 154, 3
Martin, N. F., Ibata, R. A., Irwin, M. 2007, ApJL, 668, L123
Newberg, H. J., Yanny, B., Rockosi, C., et al. 2002, ApJ, 569, 245
Price-Whelan, A. M., Johnston, K. V., Sheffield A. A., et al. 2015, MNRAS, 452, 676
Rocha-Pinto, H. J., Majewski, S. R., Skrutskie, M. F., et al. 2004, ApJ, 615, 732
Sanders, J. L. Das, P. 2018, MNRAS, 481, 4093
Schiavon, R. P., Barbuy, B., Rossi, S. C. F., Milone, A. 1997, ApJ, 479, 902
Sharma, S., Johnston, K. V., Majewski, S. R., et al. 2010, ApJ 722
Sharma, S., Bland-Hawthorn, J., Johnston, K. V., Binney, J. 2011, ApJ, 730, 3
Sheffield A.A, Price-Wheelan A. Tzanidakis A. et al. 2018, ApJ
Sheffield, A. A., Johnston, K. V., Majewski, S. R., et al. 2014, ApJ, 793, 62
Slater C. T., Bell E. F., Schlafly E. F., et al.2014, ApJ, 791, 9
Weinberg, M. D., 1995 ApJ, 455, L31

Widrow, L. M., Gardner, S., Yanny et al. 2012, ApJ, 750, L41
Xu, Y., Newberg, H. J., Carlin, J. L., et al. 2015, ApJ, 801,105
Yuan, H. B., Liu X. W., Xiang, M. S 2013, MNRAS, 430, 3